A critical trade-off between nitrogen quota and growth allows *Coccolithus braarudii* life cycle phases' to exploit varying environment

Joost de Vries[1,2], Fanny Monteiro[1], Gerald Langer[3], Colin Brownlee[2], and Glen Wheeler[2]

[1]BRIDGE, School of Geographical Sciences, University of Bristol, University Road, Bristol BS8 1SS, UK
[2]The Marine Biological Association of the United Kingdom, The Laboratory, Citadel Hill, Plymouth PL1 2PB, UK
[3]Institute of Environmental Science and Technology (ICTA), Universitat Autonoma de Barcelona, 08193 Barcelona, Spain

Correspondence: Joost de Vries (joost.devries@bristol.ac.uk)

Abstract. Coccolithophores have a distinct haplo-diplontic life cycle, which allows them to grow and divide in two different life cycle phases (haploid and diploid). These life cycle phases vary significantly in inorganic carbon content and morphology, and inhabit distinct niches, with haploids generally preferring low-nitrogen and high-temperature and -light environments *in situ*. This niche contrast indicates different physiology of the life cycle phases, which is considered here in the context of a trait trade-off framework, in which a particular set of traits comes with both costs and benefits. However, coccolithophore's phase trade-offs are not fully identified, limiting our understanding of the functionality of the coccolithophore life cycle. Here, we investigate the response of the two life cycle phases of the coccolithophore *Coccolithus braarudii* to key environmental drivers: light, temperature and nitrogen, using laboratory experiments. With this data, we identify the main trade-offs of each life cycle phase and use models to test the role of such trade-offs under different environmental conditions.

The lab experiments show the life cycle phases have similar cell size, minimum nitrogen quotas, uptake rates, and temperature and light optima. However, we find that they have different coccosphere sizes, maximum growth rates and maximum nitrogen quotas. We also observe a trade-off between maximum growth rate and maximum nitrogen quota, with higher growth rates and low maximum nitrogen quotas in the haploid phase and vice versa in the diploid phase.

Testing these phase characteristics in a numerical chemostat model, we find that the growth-quota trade-off allows *C. braarudii* to exploit variable nitrogen conditions more efficiently. Because while the diploid ability to store more nitrogen is advantageous when the nitrogen supply is intermittent, the higher haploid growth rate is advantageous when the nitrogen supply is constant.

Although the ecological drivers of *C. braarudii* life cycle fitness are likely multi-faceted, spanning both top-down and bottom-up trait trade-offs, our results suggest that a trade-off between nitrogen storage and maximum growth rate is an essential bottom-up control on the distribution of *C. braarudii* life cycle phases.

1 Introduction

Coccolithophores are important contributors to the carbon cycle. Their influence stems from their impact on the organic carbon pump through photosynthesis and the inorganic carbon pump through calcium carbonate production (Zeebe, 2012; Passow and Carlson, 2012; Boyd et al., 2019). Although both carbon pumps influence the global ocean carbon cycle, they have opposing effects. While the organic carbon pump sequesters carbon, the inorganic carbon pump releases carbon back into the atmosphere on short time scales (less than 10^4 years) (Zeebe, 2012).

Coccolithophores utilize a haplo-diplontic life cycle, which makes them distinct from other phytoplankton and allows them to grow and divide in both the haploid and diploid life cycle phases (Dassow and Montresor, 2011; Frada et al., 2018). These two life cycle phases have different inorganic and organic carbon contents, with the diploid life cycle phase generally more heavily calcified (Cros et al., 2000; Young et al., 2003; Daniels et al., 2016; Fiorini et al., 2011a, b; Frada et al., 2018). The two life cycle phases furthermore tend to have distinct niches, with the haploid cells found in lower nutrients and higher temperature and light environments (de Vries et al., 2021). These distinct niches and differences in PIC:POC ratios imply coccolithophore life cycle phases impact the organic and inorganic carbon pump differently. Nonetheless, the differential impact of coccolithophore life cycle phases is poorly understood, partly because we lack a quantitative understanding of the drivers behind the haploid and diploid distribution.

Physiology drives the growth response of phytoplankton to the environment. Understanding the physiological differences between coccolithophore life cycle phases and the subsequent impact on growth rate is thus key to understanding coccolithophore life cycle distribution. Here, we investigate the physiological differences of the coccolithophore *C. braarudii* within a trait-based framework to contextualize our results. In this framework, each trait is considered to have both costs and benefits, thus presenting trade-offs for organisms utilizing such traits (Kiørboe et al., 2018). Since trait-based approaches focus on traits rather than individual species, these results can be applied to other coccolithophore species.

Coccolithus braarudii is a key coccolithophore species in the Arctic Ocean, where it dominates coccolithophore calcium carbonate production because of its much larger size and calcium carbonate content than *Emiliania huxleyi*, which numerically dominates this region (Daniels et al., 2014). The life cycle phases of *Coccolithus braarudii* are morphologically distinct, with the haploid life cycle phase utilizing a holococcolith (HOL) morphology and the diploid life cycle phase utilizing a heterococcolith (HET) morphology (Houdan et al., 2004). Most lab work on *C. braarudii* has focused on the HET phase, with research on the HOL life cycle phase much more limited (Houdan et al., 2006; Langer et al., 2022).

The distribution of *Coccolithus braarudii* varies in the ocean with *C. braarudii* HET dominating high-nitrogen and turbulent regions, while *C. braarudii* HOL is primarily found in lower-nitrogen and more stratified regions (Malinverno et al., 2009; D'Amario et al., 2017). While some previous work suggests that differential response to turbulence (Houdan et al., 2004) and light (Langer et al., 2022) could drive this distribution difference, open questions remain about how physiology differs between the two life cycle phases.

For our experiments on *C. braarudii*, we focus on cell size, coccosphere size, nitrogen uptake rates, nitrogen quotas, and photosynthetic response (Fig. A1). These traits have been shown to influence phytoplankton distribution and can be defined

in deterministic modelling frameworks (Hansen, 1994; Hansen et al., 1997; Ward et al., 2017; Litchman et al., 2007; Follows et al., 2007; Dutkiewicz et al., 2015). For instance, cell size influences nitrogen uptake rates (Ward et al., 2017; Litchman et al., 2007), while coccosphere size influences grazing dynamics by increasing the coccolithophore diameter (Hansen, 1994; Hansen et al., 1997). Nitrogen quota influences nitrogen requirement (Litchman et al., 2007) and storage (Falkowski and Oliver, 2007; Grover, 1991). Photosynthetic response influences light optima and has previously been suggested to be a key driver in *Coccolithus braarudii* life cycle distribution (Langer et al., 2022). We also investigated differences in temperature optima, as this is a major driver of coccolithophore life cycle phases in situ (de Vries et al., 2021).

We compare changes in coccolithophore traits for three *C. braarudii* HET and three *C. braarudii* HOL life cycle phases in response to light, nitrogen, and temperature. In addition, we measure their nitrogen and DNA contents. Finally, we contextualise our results with a mechanistic model to investigate whether the trait differences provide any competitive advantage to each of the life cycle phases.

This research elucidates what fundamentally separates the two life cycle phases from a bottom-up perspective and lays the groundwork for incorporating the coccolithophore life cycle into ecosystem models.

2 Methods

2.1 Strains and culture conditions

The *Coccolithus braarudii* strains utilised in our study are the HET strains PLY182g, RCC6535, RCC1200, and the HOL strains RCC1203, RCC3777 and RCC3779. PLY182g was obtained from the Marine Biological Association (MBA) culture collection, while we obtained the rest of the cultures from the Roscoff Culture Collection (RCC). All strains were maintained using K/2 media (Probert and Houdan, 2004), which we prepared using water from the L1 station in the Plymouth sound (Smyth et al., 2010). All cultures were maintained at 15°C in a temperature-controlled room, at 50 μE m^{-2} s^{-1} under a 12:12 L:D cycle. During the experiments, all cultures were maintained in 50ml tissue culture flasks with 20ml of media. Each experiment was conducted in triplicate and in a temperature-controlled room.

Most strains were isolated near coastal regions in Europe (Fig. 1), except RCC1200, which was isolated off the coast of Namibia and RCC6535, which was isolated in New Zealand. All HOL strains were collected during the winter, while the HET strains RC6535 and RC1200 were collected in the summer. The collection date of PLY182g is unknown, but as this species tends to only occur in Plymouth during the winter (Widdicombe et al., 2010), it was likely collected during this period.

2.2 Nitrogen limitation experiments

Nitrogen limitation experiments were conducted by modifying the K/2 media from an initial NO$_3$ concentration of 220.5 μM down to to 20 μM. At this nitrogen concentration, final cell counts reached approximately 20,000 cells ml^{-1}, a cell density high enough for carbon and nitrogen analysis but low enough that we did not observe the effects of unbalanced carbonate chemistry
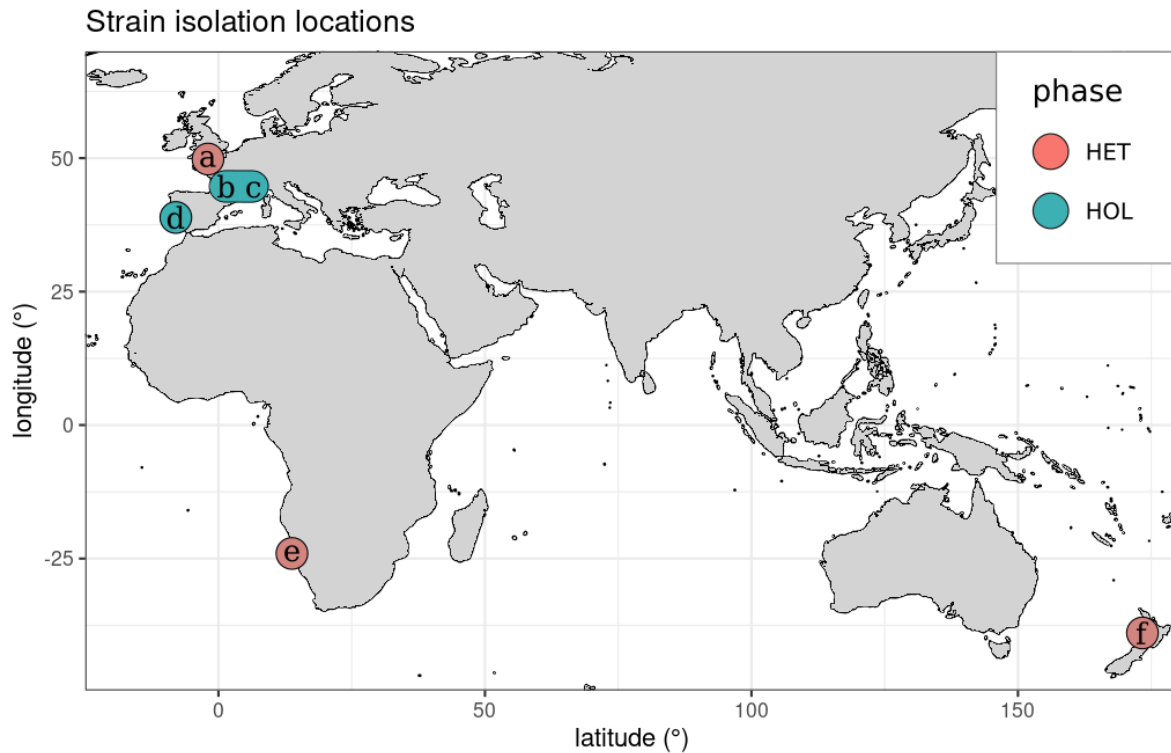
Figure 1. Isolation locations of the strains utilised in this study. The six strains investigated were: **(a)** PLY182g (HET); **(b)** RCC1203 (HOL); **(c)** RCC3777 (HOL); **(d)** RCC3779 (HOL); **(e)** RCC1200 (HET); **(f)** RCC6535 (HET).

85 (Langer et al., 2022). All nitrogen limitation experiments were conducted once the cells reached the stationary phase, assuming that the cells had drawn down all nitrogen in the media - but not other nutrients such as phosphate and trace elements.

2.3 Cell size

We measured cell size by imaging cells using a Leica DMi8 inverted microscope and analysed them using the Python package scikit-image (van der Walt et al., 2014). For each measurement, at least 100 cells were counted per strain. Specifically, we
90 segmented the images using scikit-image sobel segmentation (Kroon, 2009), and then manually sorted regions of interest by removing out-of-focus images, clusters and detritus. Assuming spherical cells, we estimated cell volume based on the mean of the longest diameters of each image.

Cell size was measured for each strain in both nutrient replete and nutrient depleted cultures. Microscopy images were taken at the same time of day (11 am) to minimise the influence of cell divisions on cell size across strains (Kottmeier et al., 2020).
95 Before imaging, the HET and HOL strains were decalcified by exposing the cultures to 1M HCL to decrease the pH to 3 and

then adding 1M NaOH to restore the pH. HOL cultures were treated for 1 minute and HET coccolithophores for 5 minutes, as we found these to be the shortest durations that decalcify the cells.

2.4 Growth rates

For replete experiments, growth rates were estimated using change in cell abundance over time as estimated using a fluorescence plate (BMG Labtech) with chlorophyll fluorescence excitation at 420 nm and at 680 nm - which were calibrated against manual Sedgewick Rafter Counter (SRC) counts. For nitrogen-replete cultures, this method worked well, with R^2 values above 0.95 for all calibrations. Growth rates for nitrogen-deplete experiments were estimated using only SRC counts, as fluorescence was found to be a poor proxy ($R^2 < 0.8$), likely due to an influence of nitrogen depletion on chlorophyll concentrations and, subsequently, fluorescence.

For each experiment, cultures were inoculated at approximately 500 cells ml^{-1} and grown until approximately 10-20k cells ml^{-1}. This initial concentration was chosen as this is near the detection limit of the fluorescence plate reader. Cell density was measured daily. The growth rate was then estimated by fitting a linear model to log-transformed counts, including only points exhibiting exponential growth and removing counts in the stationary phase.

2.5 Temperature optima

To measure the temperature response of the different strains. Each strain was grown in triplicate under nitrogen-replete conditions under 50 μE m^{-2} s^{-1} of light at 14, 15, 18, and 20°C and a 12:12 L:D light cycle. The cultures were acclimated for five generations before performing the temperature growth rate experiments. The growth rate for each temperature was measured using fluorescence with the BMG plate reader by inoculating cultures at 500 cells ml^{-1} and then measuring fluorescence daily until the cellular concentration of approximately 20,000 cells ml^{-1} was reached.

2.6 Light optima

For the light experiment, we tested seven light intensities (20, 50, 70, 100, 110, 140 μE m^{-2} s^{-1}). All light sensitivity experiments were conducted at 18°C as this was found to be the optimal temperature for all strains in our temperature-sensitivity experiments. Prior to the light sensitivity experiments, the cultures were acclimated for 5 generations. These acclimated cultures were then used to create new fluorescence-to-count calibration curves for the growth rate experiments. For the experiment, a full spectrum Kessil A360W LED with 380 and 400 nm UV bands was used, which was kept on its whitest setting and a 12:12 L:D cycle. PAR for each treatment was determined using an LI-250A Photometer (LI-COR).

Nitrogen limitation and quotas

We estimated the minimum and maximum nitrogen quotas for all five strains, called Q^{min} and Q^{max}. For Q^{max}, the maximum nitrogen content of a cell, nitrogen analysis of replete cells under exponential growth was used. This analysis was conducted by filtering the samples onto glass GF/F filters, freeze drying, and then combusting the samples in a CN elemental analyser

which was conducted by OEA Laboratories Limited (Exeter, UK). These values were then divided by cell counts to estimate cellular nitrogen concentrations.

The minimum nitrogen quota (Q^{min}), was estimated by dividing the absolute nitrogen concentration at the start of the experiment by the number of cells present once the cultures reached the stationary phase as described in Perrin et al. (2016):

$$Q^{min} = \frac{N_{init}}{cells_{fin}} \tag{1}$$

Where N_{init} is the initial nitrogen concentration and $cells_{fin}$ is the cell count at stationary phase.

2.6.1 Response of photosynthetic efficiency to nitrogen limitation

Photosynthetic efficiency (Fv/Fm) and electron transport rates (ETR) (Maxwell and Johnson, 2000) were measured using Pulse-Amplitude Modulation (PAM) for both nitrogen-replete and nitrogen-depleted cultures, which was conducted using a Walz WATER-PAM.

Fv/Fm is a measurement of maximal photochemical yield of photosystem II and is conducted by exposing dark acclimated cells to a saturation pulse of light. Changes in Fv/Fm values can represent both photodamage or enhanced radiative energy loss (a form of photoprotection). However, in practice, Fv/Fm is generally interpreted as a proxy of algal health. With non-stressed and well-acclimated photosynthetic individuals boasting higher Fv/Fm values than stressed individuals (Maxwell and Johnson, 2000). ETR is also a measure of photosynthetic yield but is measured in light-adapted cells and is a direct measurement of the quantum yield of photochemical energy conversion. Like Fv/Fm it is commonly used as a measure of stress for photosynthetic organisms (Maxwell and Johnson, 2000). Fv/Fm and ETR are computed rather than measured and thus are subject to assumptions such as equal distribution of energy across photosystem I and II and that the energy absorption is constant (Maxwell and Johnson, 2000). In theory, both of these parameters could change between the different life cycle phases, but also under nutrient limitation (e.g. which could provoke a shift in the ratio of PSI to PSII). Thus, changes in ETR could also reflect some changes in these parameters (as well as changes in the actual electron transport rate) (Gorbunov and Falkowski, 2021).

For the nitrogen-replete experiment, cultures were grown under 220 μM NO$_3$ and Fv/Fm and ETR were measured during the exponential growth phase. For the nitrogen-depleted experimental cultures, cell growth was measured daily using cell counts, and Fv/Fm and ETR were measured once cells ceased to divide. Before the Fv/Fm and ETR measurements, cells were dark acclimated for 1 hour under temperature-controlled conditions. For the measurements, Fv/Fm was taken before measuring ETR response to PAR. Measurements were taken for only PLY182g, RCC6535, RCC3777 and RCC1203. RCC1200 and RCC3779 died before the Fv/FM and ETR measurements were conducted.

In addition to ETR and Fv/Fm measurements, we also conducted ETR rapid light curves (RLC) measurements. During this experiment, samples were exposed to actinic light at 5 s intervals with increasing intensity covering 30, 100, 150, 235, 350, 530, 785, 1100, and 1500 μE m^{-2} s^{-1}. Where ETR was determined at the end of each illumination period. RLC measurements provide insight into the physiological flexibility of the cells' photosynthetic apparatus to rapid changes in light intensity.

2.6.2 DNA extraction

DNA content for each strain was measured following methods described by Liefer et al. (2019). In brief, the cultures were grown under nitrogen-replete conditions in triplicate and harvested around 20k cells ml^{-1}. The DNA was then extracted using n-lauryl sarcosine as the surfactant in the extraction protocol. It was then stained with SYBR Green II (Thermofisher S7564) and quantified using a fluorescence-based microplate analysis at 490 nm, which was calibrated against known DNA content stocks (Sigma, D4522-1MG). DNA was measured only for replete cultures.

2.7 Statistical analysis

To determine if HOL and HET cell size, coccosphere size, growth rates, DNA content, nitrogen quotas, and nitrogen uptake rates were significantly different, we conducted a two-sample t-test for each parameter. The influence of the life cycle phase on temperature and light optima was determined by fitting a generalized additive model (GAM), which included the life cycle phase as a predictor. Where, if the phase was found not to have a significant influence on model fit ($p < 0.05$), the environmental response was interpreted as not being life cycle phase specific.

Analysis was conducted in R, and the t-test was conducted with the "stats" package (R Core Team, 2022), while the GAM analysis was done with the "mgcv" package (Wood, 2011). Before fitting each GAM, growth data was Min-Max normalized for each species individually to remove the influence of ploidy-specific maximum growth rate differences.

2.8 Modelling

Nitrogen uptake experiments are tedious and expensive using reactor experiments. We thus follow an alternative strategy as proposed by Perrin et al. (2016) fitting models to batch culture experiments to derive the parameters. Our modelling strategy in this manuscript is thus twofold: first, we fit a model to experimental data to derive nitrogen uptake parameters. We then use this data for a second model, simulating resource competition of the two life cycle phases under different nitrogen conditions and physiological parameterisations (so-called 'sensitivity experiments').

2.8.1 Model for nitrogen uptake estimations

Mechanistic modelling relies on our understanding of cellular physiology to represent cell growth and nitrogen limitation processes. This can be done with varying degrees of complexity ranging from simple models such as the Monod model, which assumes a direct relationship between nitrogen concentrations and growth rates (Monod, 1949), to very complex models such as that by Inomura et al. (2020), which represent individual cellular processes such as nitrogen storage, transfer and reorganisation of cellular machinery. Here we utilise an internal quota cellular model, an intermediate complexity mechanistic model, which accounts for cellular nitrogen storage but does not trace individual cellular processes. Such models can take several forms, including Droop and linear models as described in detail in Flynn (2008). Here we employ the normalised rectangular hyperbolic (RH) model as proposed by Flynn (2002), which includes a response variable, which modulates the relationship between nitrogen quota and growth.

Conceptually, the RH internal nitrogen model regulates growth rates based on the available internal nitrogen, which depends
190   on the nitrogen uptake rate and the concentration of external nitrogen (Eq.2-7). The model traces environmental nitrogen
concentration (N, μmol l^{-1}), the cellular concentration (P, cells l^{-1}), and the internal nitrogen quota (Q, μmol cell^{-1}) using
the following three differentials:

$$\frac{dP}{dt} = \mu \cdot P \tag{2}$$

$$\frac{dN}{dt} = -V \cdot P \tag{3}$$

195    $$\frac{dQ}{dt} = V - \mu \cdot Q \tag{4}$$

where μ is the growth rate (d^{-1}) and V is the nitrogen uptake rate (μmol cell^{-1} d^{-1}).

The modelled growth rate μ depends on the nitrogen quota, which we define here following Flynn (2002)'s RH formulation:

$$\mu = \mu^{max} \cdot \frac{(1 + KQ)(Q - Q^{min})}{(Q - Q^{min}) + KQ(Q^{max} - Q^{min})} \tag{5}$$

where μ_{max} (d^{-1}) is the maximum growth rate under nitrogen-replete conditions, Q^{min} (pgN cell^{-1}) is the minimum
200   cellular nitrogen quota, Q^{max} (pgN cell^{-1}) is the maximum cellular nitrogen quota, and KQ is a dimensionless parameter that
determines the relationship between the internal nitrogen quota and growth rate.

We estimate KQ based on Q^{min} and Q^{max} as defined by Flynn (2008):

$$KQ = \frac{Q^{min}}{Q^{max} - Q^{min}} \tag{6}$$

In this equation, strains with a small ratio of minimum to maximum nitrogen quotas have a strong linear relationship between
205   growth rate and nitrogen quota. While strains with a large minimum to maximum nitrogen quota ratio exhibit a non-linear
relationship between nitrogen quota and growth (Flynn, 2008).

The cellular nitrogen quota (Q) is replenished based on the cellular nitrogen uptake rate, which we define here using
Michaelis-Menten uptake kinetics, while also limiting uptake when the cellular nitrogen quota is full:

$$V = V^{max} \cdot \frac{[N]}{[N] + K_N} \cdot \frac{Q_i^{max} - Q_i}{Q_i^{max} - Q_i^{min}} \tag{7}$$

210   where, V_{max} is the per cellular nitrogen uptake rate (in μmol$_R$ cell^{-1} d^{-1}) and K_N is the Michaelis-Menten half-saturation
constant (in μmol l^{-1}).

2.8.2 Estimating nitrogen uptake rate using the internal storage model

The internal stores model used in our study includes six key parameters (see Eq. 2-7): μ^{max}, V^{max}, Q^{min}, Q^{max}, K_N and KQ (Table 1). We empirically measured and estimated Q^{min} and Q^{max} from our lab experiments (see Section 2.6). The other parameters were estimated through previously described relationships or fitting models to our lab data, as this approach is cost and time-effective and works well (Perrin et al., 2016). We calculated KQ using Eq. 6 and approximated μ^{max}, V^{max} and K_N using the models described below.

2.8.3 Maximum growth rate

We estimated the maximum growth rate (μ^{max}) by fitting the sigmoidal function described by Zwietering et al. (1990) and Ward et al. (2017) to our nitrogen limitation experiment data.

$$y = \frac{A}{1 + \exp[(4\mu^{max}/A)(\lambda - t) + 2]} \tag{8}$$

where A is the log of the maximum cell density (cells ml^{-1}) observed in the experiment, λ is the lag time (d^{-1}) defined as the time the tangent to the curve at its inflection point equals 0.

2.8.4 Maximum nitrogen uptake rate

We estimated the maximum nitrogen uptake rate (V^{max}) for each strain by simplifying the equation proposed in Verdy et al. (2009):

$$\mu^{max} = \frac{\mu^{\infty} V^{max}(Q^{max} - Q^{min})}{V^{max} Q^{max} + \mu^{\infty} Q^{min}(Q^{max} - Q^{min})} \tag{9}$$

Assuming that the realized maximum growth rate (μ^{max}) approximates the theoretical maximum growth rate (μ^{∞}) as proposed by Ward et al. (2017) for cells $>10\mu$m and re-arranging Eq. 9 for V^{max} lead to the equation:

$$V^{max} = \frac{\mu^{max} Q^{min}}{1 + Q^{min}} \tag{10}$$

2.8.5 Maximum nitrogen uptake rate

For the remaining unknown parameter, the half-saturation constant for nitrogen uptake (K_N), we used a non-linear least squares fitting procedure to fit the internal nitrogen stores model to our laboratory data. This fitting was conducted by minimising error through 'Basin-Hopping' of mean squared errors calculated for each set of parameter estimations (Wales and Doye, 1997). Basin-Hopping was conducted with the 'basinhopping' function in Python from the scipy.optimise library (Virtanen et al., 2020).

We constrained K_N to be positive as empirically, the half-saturation constant for growth cannot be negative. This was done by forcing the mean squared error value to infinity if bounds were not met (a high mean squared error value indicates a bad fit). Bounds for K_N were defined the same for all strains and set to be between $1e^{-99}$ and $1e^{99}$. Initial fitting K_N estimates were based on *Emiliania huxleyi* data from Perrin et al. (2016) and set to values of $0.35\ \mu\text{mol}\,l^{-1}$.

2.8.6 Chemostat model

To better visualise and interpret the impact of the different nitrogen dynamics of the different coccolithophore strains, we developed a numerical 'chemostat' model. This model simulates resource competition between the HET and HOL strains, differentiated by their maximum growth rates and nitrogen storage, as observed in the lab experiments.

For our chemostat model, we forced fluxes of nitrogen concentration using a pulse wave, which we define using a Fourier series expansion:

$$N(t) = A\frac{\tau}{T} + \frac{2A}{\pi}\sum_{n=1}^{\infty}\left(\frac{1}{n}\sin\left(\pi n\frac{\tau}{T}\right)\cos\left(2\pi n\frac{1}{T}t\right)\right) \tag{11}$$

where A is the pulse amplitude (μM), τ is the pulse length (d^{-1}), T is the pulse period (d^{-1}), t is time (d), and n (unitless) is the integer multiple (which determines the "squareness" and is set as 100).

To model phytoplankton abundance of both HET and HOL strains in our model, we follow the equations described in Follows et al. (2018). However, we imposed a quadratic mortality term m (d^{-1}) to represent viral lysis, grazing pressure and sinking as this is proposed to be more realistic (Steele and Henderson, 1992). We also included a chemostat turn-over term κ (d^{-1}). In this model cell concentration of a given phytoplankton i is:

$$\frac{dP_i}{dt} = \mu_i P_i - \kappa P_i - mP_i^2 \tag{12}$$

The growth rate (μ_i) in this model follows the Flynn (2002) internal nitrogen model as described in Eq. 4.

Following Follows et al. (2018), we modelled the internal nitrogen quota for a given phytoplankton i as a function of nitrogen uptake rate and growth with a quadratic mortality term:

$$\frac{dQ_i}{dt} = V_i - \mu_i Q_i - mQ_i^2 \tag{13}$$

where V_i is limited as the quota approaches the maximum value to prevent excess nitrogen accumulation following Eq. 6.

For all our numerical experiments, we used the Python Scipy 'solve_ivp' function to integrate the system of ordinary differential equations using the RK45 algorithm described by Dormand and Prince (1980).

2.8.7 Sensitivity experiment

Using the chemostat model, we explored the sensitivity of the maximum nitrogen quota (Q^{max}), as this is the main trait difference observed between the HET and HOL strains across our temperature, light and nutrient experiments.

265   Mechanistically, a high Q^{max} relates directly to nitrogen storage and, in theory, benefits the organism when nitrogen supply is intermittent. Following the trait-based theory, Q^{max} should also have a cost; otherwise, it would lead to the evolution of 'superorganisms' out-competing everything else (Follows and Dutkiewicz, 2011). Among the potential costs of nitrogen storage, the metabolic cost seems the most compelling cost since Q^{max} is inversely related to maximum growth in our lab results, and as specified by previous literature (Grover, 1991).

270   We thus explored the competitive advantage of a higher Q^{max} under different nitrogen intermittence input regimes, testing nitrogen concentrations ranging from steady states to inputs only once every four days. We did this by comparing relative HET and HOL abundances under different input scenarios with and without a metabolic cost of nitrogen storage (Table A2). Metabolic cost was implemented as a reduced maximum growth rate for HET strains, which have a higher Q^{max} value. Reduced growth rate values for the metabolic cost experiment were chosen based on those observed in our experiments with

275 HET cells assigned a maximum growth rate of 0.5 d^{-1} while the HOL cells were assigned a maximum growth rate of 0.7 d^{-1}. Each competition experiment was run until relative abundances reached a steady state. Nitrogen concentration was kept constant and above saturation - although the exact nitrogen concentration did not impact relative abundances since K_N and V^{max} values were defined to be the same for both life cycle phases.

3   Results

280 ### 3.1   Cell and coccosphere size

Under maintenance conditions (15°C, μE m^{-2} s^{-1}) , all *C. braarudii* strains have a similar cell diameter (with a mean diameter of 18.2 ± 0.8 μm) (Fig. 2a) with no significant difference between HOL and HET strains (p-value = 0.195). However, a significantly larger coccosphere size is observed for the HET strains (23.8 ± 2.4 μm) compared to the HOL strains (19.5 ± 2.2 μm, p-value < 0.001) (Fig. 2b).

285 ### 3.2   Light and temperature optima

Our lab experiments showed that all strains have a temperature optimum at 18°C with a steep decline in growth at higher and lower temperatures (Fig. 3a). There is no significant difference in temperature optima between the two life cycle phases, as shown in our generalized additive model (p-value = 0.061).

     Response to light was found to be strain-specific (Fig. 3b), with no significant differences between the different life cycle

290 phases (p-value = 0.383). For example, only HET PLY182g and HOL RCC1203 display growth inhibition at 150 μE m^{-2} s^{-1}, while the other strains do not. We note that our tested irradiance values are much lower than potentially experienced in situ, which can reach over 1,000 μE m^{-2} s^{-1} in surface waters (Laliberté et al., 2016).

a) Cell diameter
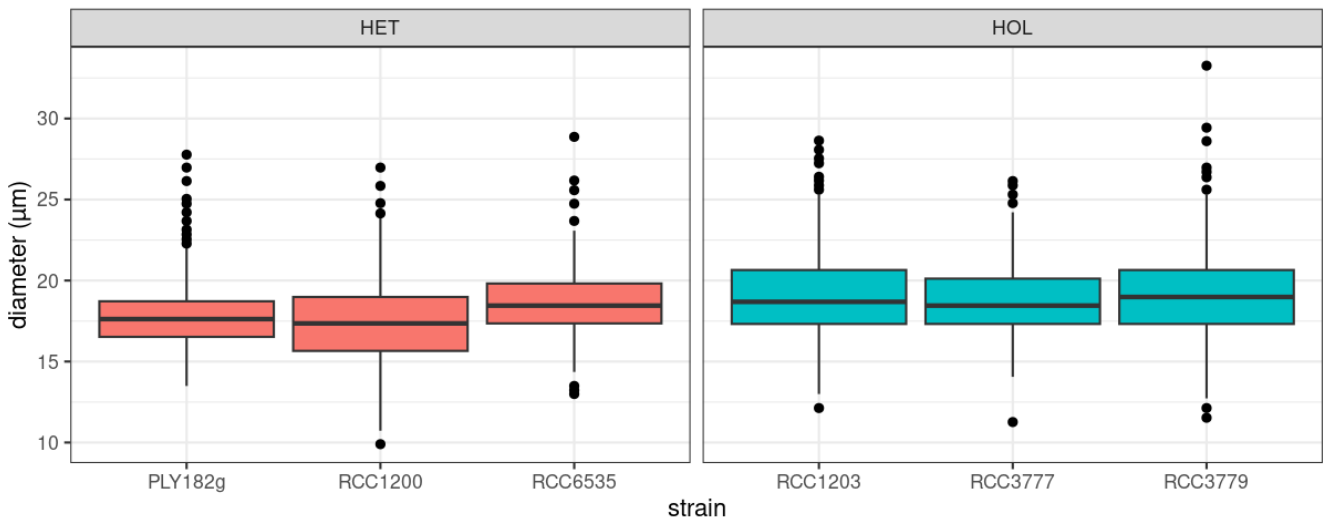
b) Coccosphere diameter
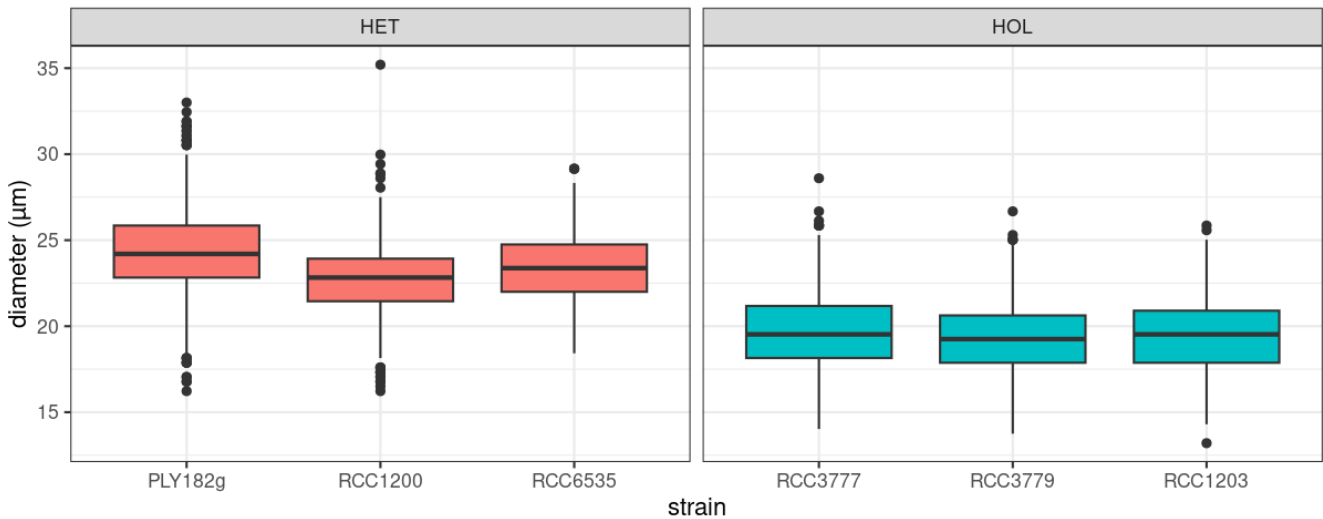
Figure 2. Comparison of cell and coccosphere sizes in cultured *C. braarudii* strains (N=100). Diameters of: **(a)** cells and **(b)** coccospheres (μm) as measured by light microscopy imaging.

3.3 Maximum specific growth rates

Our light and temperature optima experiments suggest that overall HOL maximum growth rates (0.73 ± 0.07 d^{-1}) are significantly higher than HET maximum growth rates (0.56 ± 0.07 d^{-1}, p-value < 0.001; Fig. 4).
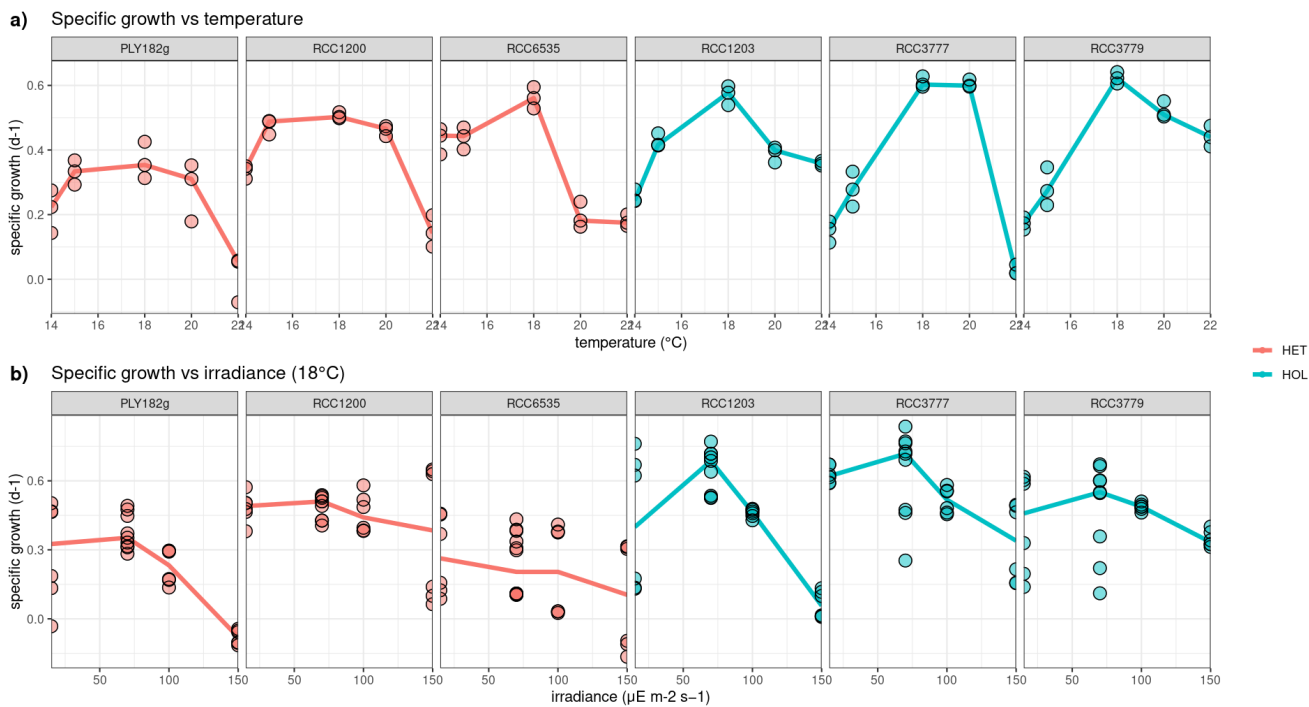
Figure 3. Temperature and Irradiance optima of *C. braarudii* HET and HOL strains. Optima for: **(a)** temperature and **(b)** irradiance. N=3 for each boxplot.

3.4 Photosynthesis and nitrogen limitation

To test the response of nitrogen limitation on photosynthetic response, we measured HET and HOL cultures under nitrogen-replete and depleted conditions under maintenance conditions ($15°C$, $\mu E\ m^{-2}\ s^{-1}$). During the nitrogen repletion experiments, HET and HOL cells displayed similar maximal photosynthetic efficiency (Fv/Fm), (p-value = 0.056) and higher Electron Transport Rates (ETR; p-value = 0.004). When nitrogen-limited, both HET and HOL strains exhibit a reduced Fv/Fm (Fig. 5). However, this inhibition is significantly higher during the nitrogen-depleted conditions for the HOL strains than for the HET strains (p-value < 0.001). Furthermore, the HOL phases show highly reduced ETR during photosynthesis, especially when exposed to high light. These results suggest that the HOL life cycle phase allocates less resources towards its photosynthetic machinery when nitrogen-limited, reducing its photosynthetic efficiency and increasing its light inhibition sensitivity. This contrasts with the HET strains, which can maintain high photosynthetic efficiency when nitrogen-depleted.
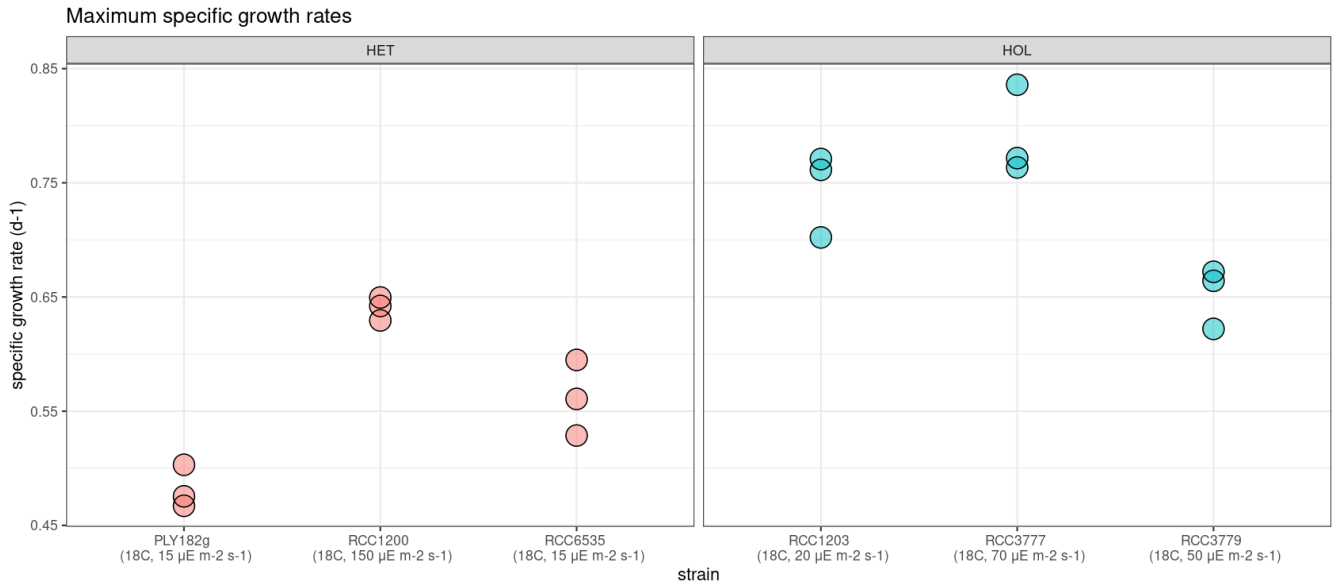
Figure 4. Maximum specific growth rates (d^{-1}) of *C. braarudii* strains at their respective temperature and light optima (N=3). Note that higher maximum specific growth rates are observed for HOL strains.

3.5 Nitrogen and genome content

We find that the HET life cycle phase contains twice the DNA content of HOL (Fig. A2), indicating that all strains have a similar genome size and ploidy drives the variations in genome content for the HET and HOL strains investigated in this study. Under nitrogen-replete conditions (Fig. 6a), the genome content accounts for 5-15% $(10.7 \pm 5.8 \text{ \%})$ of the nitrogen budget, varying with the strains and with no significant difference between the phases (Fig. 6b). This percentage is similar to what is observed in diatoms, other algae, and cyanobacteria (Liefer et al., 2019; Geider and Roche, 2002). Notably, however, the minimum nitrogen quotas of the HET and HOL coccolithophore strains are very similar under nitrogen-depleted conditions, with no significant difference between the observed HET and HOL cells (p-value = 0.985). Thus for HET to maintain a similar nitrogen quota under nitrogen-depleted conditions, they must restrict other cellular resources. However, what part of the nitrogen demand HET strains reduce is not clear.

3.6 Nitrogen uptake rates and half-saturation constants

All strains show similar half-saturation constants (K_N), maximum nitrogen uptake rates (V^{max}), maximum growth rates (μ^{max}), and minimum nitrogen quotas (Q^{min})(Table 1, Fig. A1). Furthermore, there is no apparent difference between the HET and HOL life cycle phases (Fig. A2).
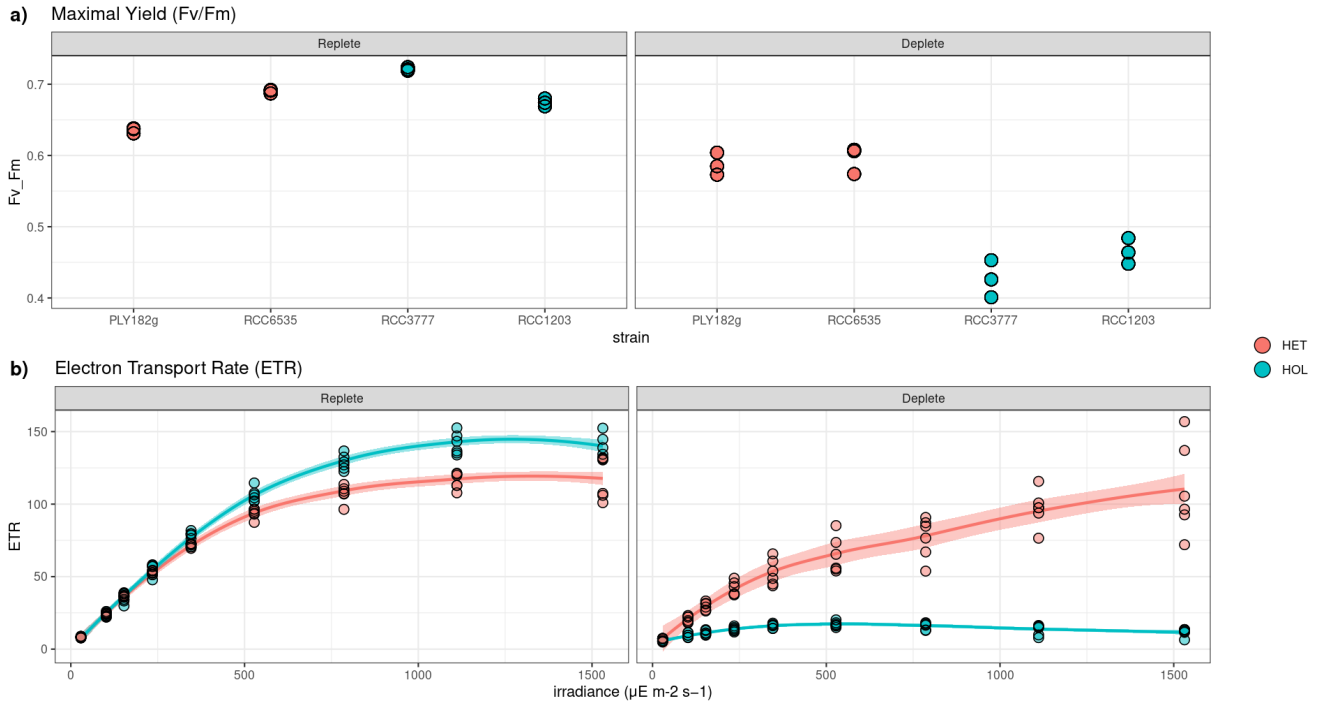
Figure 5. Response of photosynthetic machinery to nitrogen limitation measured by pulse amplitude measurements (PAM). **(a-b)** Maximal yield (Fv/Fm); **(c-d)** Electron Transport Rate (ETR) in response to PAR. ETR results show the average values of the HET and HOL strains

320   The only noticeable difference observed in our nitrogen parameter estimates are maximum nitrogen quotas (Q^{max}), which was significantly higher for HET strains (34.0 ± 11.1 pgN cell^{-1}) compared to HOL strains (66.1 ± 17.7 pgN cell^{-1}, p-value < 0.001).

strain	phase	μ^{max} (d^{-1})	Q^{min} (pgN cell^{-1})	Q^{max} (pgN cell^{-1})	V^{max} (μmol cell^{-1} d^{-1})	K_N (μmol l^{-1})	KQ (unitless)
PLY182g	HET	0.50	21.68	53.57	$2.14 \cdot 10^{-4}$	1.14	0.68
RCC1200	HET	0.65	23.53	78.57	$2.43 \cdot 10^{-4}$	1.21	0.43
RCC3777	HOL	0.83	18.45	21.43	$1.67 \cdot 10^{-4}$	1.50	6.20
RCC3779	HOL	0.67	17.11	38.57	$2.440 \cdot 10^{-4}$	1.18	0.80
RCC1203	HOL	0.77	27.56	42.14	$2.44 \cdot 10^{-4}$	0.96	1.89

Table 1. Model parameters for the five strains tested. Maximum growth rate (μ^{max}), minimum nitrogen quota (Q^{min}), maximum nitrogen quota (Q^{max}), maximum nitrogen uptake rate (V^{max}), nitrogen half saturation constant (K_N), ratio between minimum and maximum nitrogen quota (KQ).
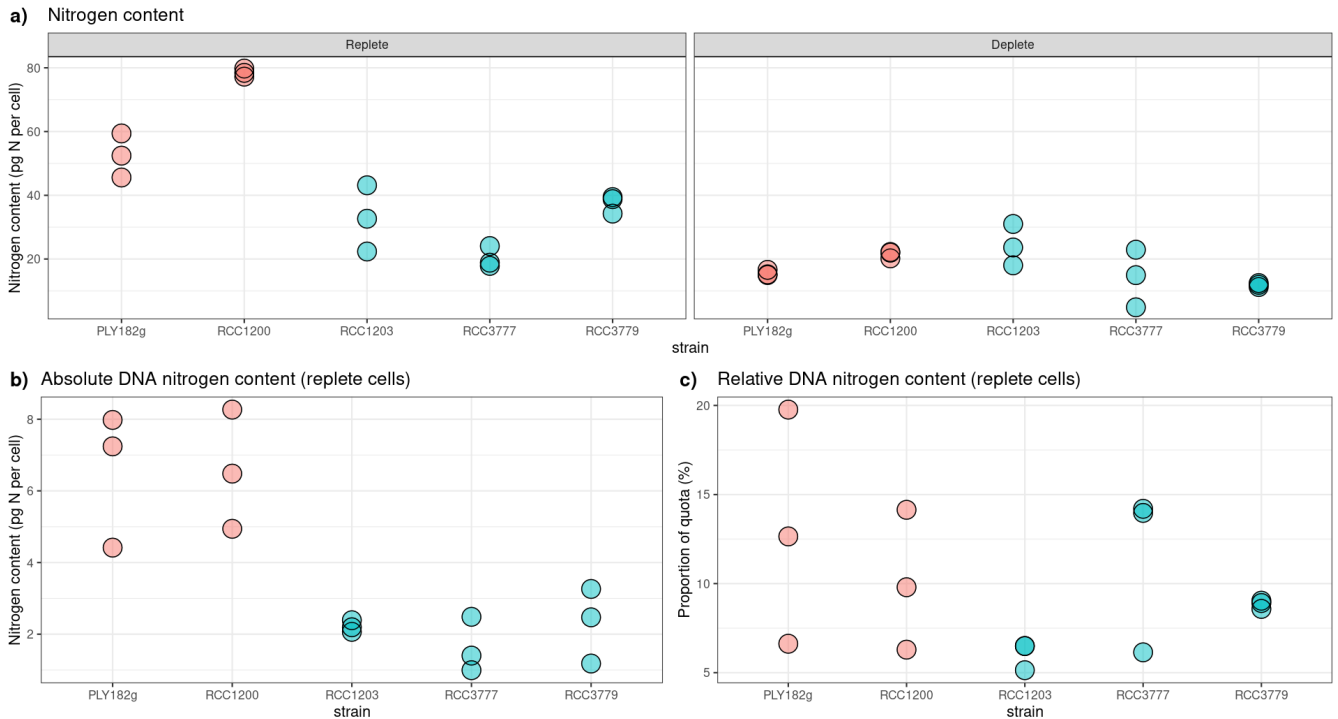
Figure 6. Nitrogen and genome content per strain under replete and depleted nitrogen conditions. **(a)** Cellular nitrogen quota, where replete quota is equal to Q^{max} and depleted quota is equal to Q^{min}; **(b)** DNA content relative to nitrogen content.

3.7 Trait trade-offs

Overall, the only significant differences we observe between the HET and HOL strains are the coccosphere size, the maximum nitrogen quota (Q^{max}) and the maximum growth rate (μ^{max}). Following trait-based approaches, we argue that the trait trade-offs for *C. braarudii* likely relate to those three trait characteristics. Of these traits, both trade-offs between calcification status and growth and maximum nitrogen quota and growth are plausible (Grover, 1991; Monteiro et al., 2016). However, as the influence of calcification status on growth is not noted in previous literature (Houdan et al., 2005), and we do not have PIC estimates of the HOL cells due to difficulties of making such estimates (Langer et al., 2022), we focus here on the implication of a maximum nitrogen quota and growth rate trade-off.

3.8 Numerical simulation experiments

Our numerical simulations compared the ratio between HET and HOL cells due to different relative maximum nitrogen quota (Q^{max}) values as measured in our lab experiments (Fig. 7). Where HET cells contributed a higher proportion, this was inter-

preted as a higher competitive advantage of nutrient storage. We test the advantage of a higher nutrient storage (Q^{max}) with no
335 cost (Fig. 7a), and with reduced growth rate (0.5 and 0.7 d^{-1} for the HET and HOL cells, respectively).
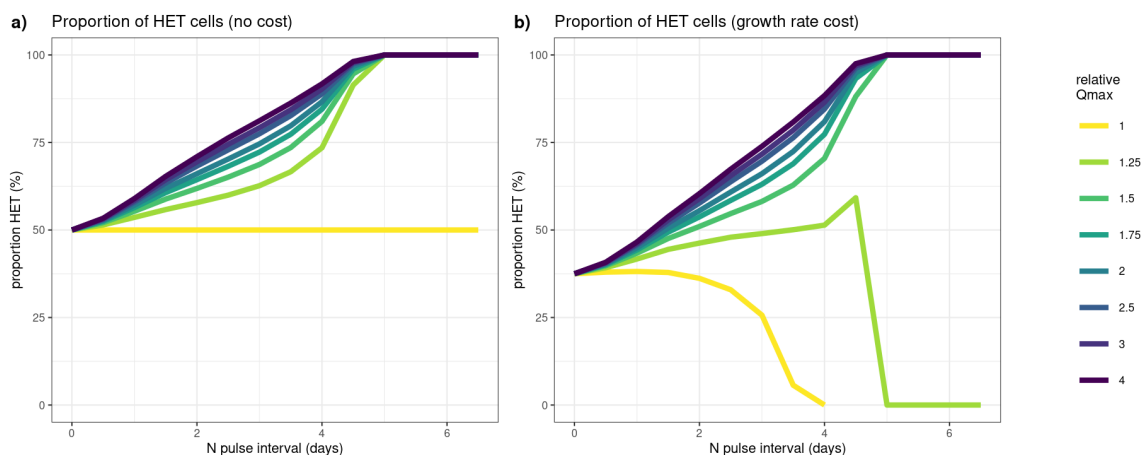
Figure 7. Results of our numerical simulation experiments. Here we test how different values of maximum nitrogen quotas (Q^{max}) effect competition of HET and HOL cells under varying nitrogen pulses (N pulse interval). **(a)** Assuming no cost of a higher nitrogen quota (equal growth rates, μ^{max}); **(b)** Assuming a cost on growth rate where HET cells have a lower maximum growth rate (μ^{max} = 0.5 d^{-1}) and HOL cells have a higher maximum growth rate (μ^{max} = 0.7 d^{-1}). Different ratios of maximum nitrogen quotas were tested for each scenario, where relative Q^{max} is the ratio between HET and HOL Q^{max}. E.g. a value of 2 denotes a HET Q^{max} twice the size of the HOL Q^{max}. The y-axis in both plots denotes the proportion of diploid cells relative to the number of haploid cells.

Both sensitivity model experiments show a clear advantage of having high Q^{max} with intermittent nitrogen supply with and without a growth rate cost (relative Q^{max}; Fig. 7). However, this advantage decreases when nitrogen input is close to constant, or when the relative Q^{max} is low and nitrogen input is intermittent (Fig. 7b).

With a relative Q^{max} between HET and HOL of *C. braarudii* of around 2 as measured in our lab study, the model shows
340 that HET cells can be more competitive under nitrogen intermittent regimes despite their lower observed growth rates.

4   Discussion

Our results generally agree with previous measurements made of *C. braarudii*. For our Q^{max} estimates of PLY182g, we observe a PON of 54 pgN cell^{-1}, compared to a PON value to 40.6 pgN cell^{-1} reported in Villiot et al. (2021). While for RCC1200, we observe a PON of 78.57 pgN cell^{-1}, compared to a value of 94.8 pgN cell^{-1} in Gerecht et al. (2014). While there is no
345 direct comparison for K_N, the K_N value of 1.06 μM reported by Cermeño et al. (2011) for strain RCC1201 is similar to our estimates of 1.14 μM and 1.21 μM for PLY182g and RCC1200, respectively. In terms of response to irradiance, compared to the work by (Langer et al., 2022), we notice stronger growth inhibition from 150 μE m^{-2} s^{-1} for the strain PLY182g. This difference could be due to experimental temperature differences, with our experiment conducted at 18°C instead of 15°C. The

difference could also be due to the difference in light sources used in the two experiments, as we used an LED light with a UV band (390 to 400 nm) instead of the fluorescent light source with no UV used in Langer et al. (2022). Nonetheless, the trends in our study for the two strains are similar to those reported by Langer et al. (2022), with PLY182g HET showing a more potent light inhibition than RCC3777 HOL. Here, by analyzing a series of strains, we find this difference is strain- and not ploidy-specific, as both HET and HOL life cycle phases exhibit differences in response to irradiance. Finally, our maximum growth rates of 0.5 for HOL and 0.7 for HET also agree well with Langer et al. (2022), who reports maximum growth rates of 0.5 and 0.9 for PLY182g HET and RCC3777 HOL, respectively.

While our study expands on previous work considering only single strains, we are nonetheless limited by the strains utilized in this study, in particular, because the HET and HOL life cycle phases used are not from the same strain and are collected at different sampling locations. Furthermore, all strains were collected at coastal areas, with none in open ocean locations. Follow-up experiments conducted with HET and HOL life cycle phases of the same strain and studies on strains collected in the open ocean would thus be very informative in further elucidating the differences we observe here.

Nonetheless, by utilizing multiple strains and considering multiple traits in parallel, we expand on previous literature by showing that higher nitrogen quotas and the ability to deal with varying pulsed nitrogen regimes may be a main bottom-up control of the distribution of *C. braarudii* life cycle phases, with diploid *C. braarudii* investing more into nitrogen storage at the cost of lower growth rates but with the benefit of being able to deal with more intermittent nitrogen supplies. This result suggests that lower nitrogen intermittence during summer stratification rather than differences in nitrogen concentration could cause the in situ seasonal variation in HET and HOL coccolithophores observed in situ (de Vries et al., 2021), including *C. braarudii* (Malinverno et al., 2009; D'Amario et al., 2017).

Furthermore, previous studies also identified nutrient storage as an important driver of phytoplankton distribution in the modern ocean (Falkowski and Oliver, 2007; Grover, 1991), with turbulence affecting nutrient inputs (Falkowski and Oliver, 2007; Grover, 1991; Tozzi et al., 2004). While turbulence and nutrient input are not strictly the same process, they are generally considered as such in previous modelling experiments and literature (Falkowski and Oliver, 2007; Grover, 1991; Tozzi et al., 2004) and are used interchangeably here.

Besides, nutrient storage relates to functional types, with a succession of nutrient storage ability observed for diatoms, coccolithophores and dinoflagellates (Margalef, 1978). For example, diatoms boast highly specialised nutrient storage vacuoles compared to dinoflagellates (Lomas and Glibert, 2000), which allows diatoms to exploit intermittent nutrient regimes better. Furthermore, differences in nutrient storage may influence the evolution and distribution of diatoms and coccolithophores on geological time scales (Tozzi et al., 2004). For instance, the early Panthalassa (250-190 Ma) and associated lower global turbulence seem to have favoured coccolithophores, while in the modern day, greater turbulence globally favours diatoms (Tozzi et al., 2004).

The potential role nutrient storage and turbulence play in determining phytoplankton distribution across geological time scales are interesting when contextualised with the idea that the haplo-diplontic life cycle of coccolithophores allows single species to expand their niche in the modern ocean (de Vries et al., 2021). This concept suggests that the coccolithophore life cycle might also prevent extinction across geological time scales, allowing adaptation toward a larger range of nutrient regimes.

Differences in turbulence preference are also notable in the context of coccolithophore success during anthropogenic climate change, as climate models predict increased stratification in our near future oceans (Fu et al., 2016)

The advantage of higher nutrient quotas comes from the ability to withstand more extended periods without nutrients and longer periods at which maximum uptake rate (V^{max}) is sustained, as it takes longer for the quota to be satiated. Previous works by Verdy et al. (2009) and Grover (1991) suggest that a positive relationship between maximum uptake rates and higher nutrient quotas primarily drives this. However, here we illustrate that this effect occurs even when V^{max} is similar, as even with the same V^{max} values, it takes longer for the quota to reach maximum values if Q^{max} is high.

Besides HET's higher nitrogen storage ability, we furthermore observe significantly reduced photosynthetic ability for HOL cells in nitrogen-depleted conditions compared to HET cells. Although we do not explicitly model this effect, this could further differentiate the competitiveness of HOL coccolithophores when experiencing intermittent nitrogen supplies.
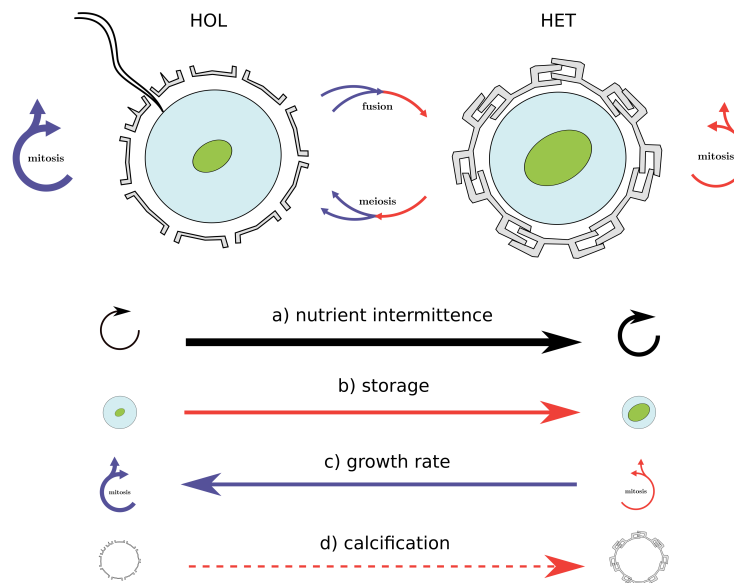
Figure 8. Nitrogen intermittence trait trade-offs of the *C. braarudii* life cycle. This study identifies a nitrogen quota and growth trade-off as a key driver for differences in HET and HOL *C. braarudii* distribution. While the investment of HET cells into comparatively higher nitrogen storage comes at the cost of lower growth rates, this disadvantage is overcome when nitrogen supply is intermittent. Likewise, HOL cells out-compete HET cells when the nitrogen supply is constant due to higher growth rates but are out-competed when the nitrogen supply becomes intermittent. Other potential but theoretical competitive advantages under different nitrogen regimes not considered in our model includes calcification state (d), which also varies between HET and HOL *C. braarudii* cells.

Finally, while we observe similar cell sizes of HET and HOL life cycle phases, a larger coccosphere size for HET life cycle phases is observed. The similarity in cell diameter but not in coccosphere size between the two life cycle phases suggests that the phases have the same size trait trade-off from a nitrogen perspective but a different trait trade-off regarding grazing

susceptibility. The coccosphere volume does not impact nitrogen uptake dynamics on the first order since it does not increase the cell surface area but may impact grazing dynamics. Higher grazing protection of more heavily calcified HET life cycle phases might also be closely related to turbulence, as highly turbulent regimes are associated with higher predator encounters (Kiørboe, 1997). Furthermore, higher sinking rates associated with higher calcification states (Bach et al., 2012) might be unfavourable in highly stratified regions.

While our work focuses on nitrogen storage and the subsequent ability to deal with different nitrogen-input regimes, other trait differences, such as calcification, and traits not considered in this study, such as motility (Frada et al., 2018) and phagotrophy (Rokitta et al., 2011; Avrahami and Frada, 2020), means the full trait-trade-off space of *C. braarudii* is difficult to constrain. Further model-based sensitivity analysis of such trait trade-offs in more complex ecosystem models could thus be useful in determining the role some of these other traits play. For example, in the context of our lab results, the impact of coccosphere size on grazing susceptibility without accounting for additional predator-prey effects could already be very informative in determining the role this might play on distribution dynamics.

Our study shows that the genome content of HET cells is twice that of HOL cells, but that, nonetheless, the nitrogen quotas of both phases are similar when nitrogen deplete, which suggests that the presence of other trade-offs not considered here might be essential in sustaining similar minimum nitrogen quotas for HET and HOL cells. While the nitrogen contribution of the genome is small, previous work has shown that for another coccolithophore species, *E. huxleyi* genome content is a selective pressure in oligotrophic environments (Dassow et al., 2015). In such regions, multiple environmental isolates of this species have lost genes associated with the HOL life cycle phase and are therefore stuck in the HET phase (Dassow et al., 2015). However, a more thorough macromolecular analysis is necessary to elucidate which budgets diploid cells are reducing to make up for a higher nitrogen cost of the diploid genome. For this, proteomics would be particularly useful as it constitutes most of the nitrogen budget of phytoplankton (Liefer et al., 2019).

Furthermore, our research focuses primarily on nitrogen storage and uptake dynamics, but phosphate is also critical in regulating global phytoplankton distribution (Tyrrell, 1999). The role of phosphate storage plays in HET-HOL competitive dynamics thus also warrants further research, particularly as, unlike nitrogen, phytoplankton cells utilise phosphate-specific storage bodies in the form of polyphosphate (Liefer et al., 2019), which for coccolithophores is tied to calcium storage (Sviben et al., 2016; Gal et al., 2018).

5   Conclusions

Using an integrated approach featuring both laboratory experiments and numerical simulations, we find that *C. braarudii* life cycle phases have different nitrogen storage and maximum growth rates, but similar light preference, nitrogen uptake rates and temperature optima. The maximum growth is inversely related to nitrogen storage, with HOL having higher growth rates and lower nitrogen storage and HET having lower growth rates and higher nitrogen storage. This result indicates a potential trade-off between growth and nitrogen storage, which could be a primary bottom-up control of *C. braarudii* life cycle phase distribution.

430   Higher nitrogen storage allows HET coccolithophores to better exploit regimes of intermittent nitrogen supply, such as highly turbulent regions. This benefit comes at the cost of a lower competitive ability due to a lower maximum growth rate when turbulence is low, and nitrogen supply is constant.

The *C. braarudii* HET life cycle phase's ability to better store nitrogen is also associated with high photosynthetic efficiency when the cell experiences nitrogen depletion further suggesting an important role of photosynthesis during nitrogen depletion.

435   We found that genome content plays a minor role in the nitrogen budget of nitrogen-replete cells, but that the absolute DNA content is higher for HET cells. Notably, this higher genome content does not correlate with higher minimum nitrogen quotas for HET cells, suggesting that HET cells reduce other cellular components to maintain similar minimum nitrogen quotas. However, as we can not infer such budget cuts, our work highlights that more thorough macromolecular investigations of the HET-HOL life cycle phases are warranted.

440   Overall, our work shows the advantage of studying the coccolithophore life cycle in a trait-based framework. By comparing differences in traits between the different life cycle phases, we identify the key traits that determine the distribution of coccolithophore phases. This work furthermore provides parameterisations needed for more in-depth numerical simulations and analysis, which provides an exciting avenue for future coccolithophore life cycle research.

Code availability. The HET-HOL competition model is available on figshare: 10.6084/m9.figshare.22717873.

445   *Author contributions.* JdV, GW and FM conceptualized the manuscript. JdV, GW and GL conceptualized the lab experiments. JdV and FM conceptualized the numerical simulations. JdV performed the lab experiments, developed the competition model, conducted the formal analysis, and visualized the results. JdV, GW, FM, GL and CB interpreted the results. JdV, GW and FM prepared the manuscript with contributions from all co-authors.

Competing interests. The authors declare that they have no conflict of interest.

450   *Acknowledgements.* This research has been supported by a NERC GW4+ DTP studentship (grant nos. NE/L002434/1) to JDV, the National Environmental Research Council grant nos. NE/X001261/1 to FM and NE/N011708/1 to GW; the European Research Council (SEACELLS, grant no. 670390) to CB; and funding from the Spanish Ministry of Education through a Maria Zambrano grant to GL.

Appendix A
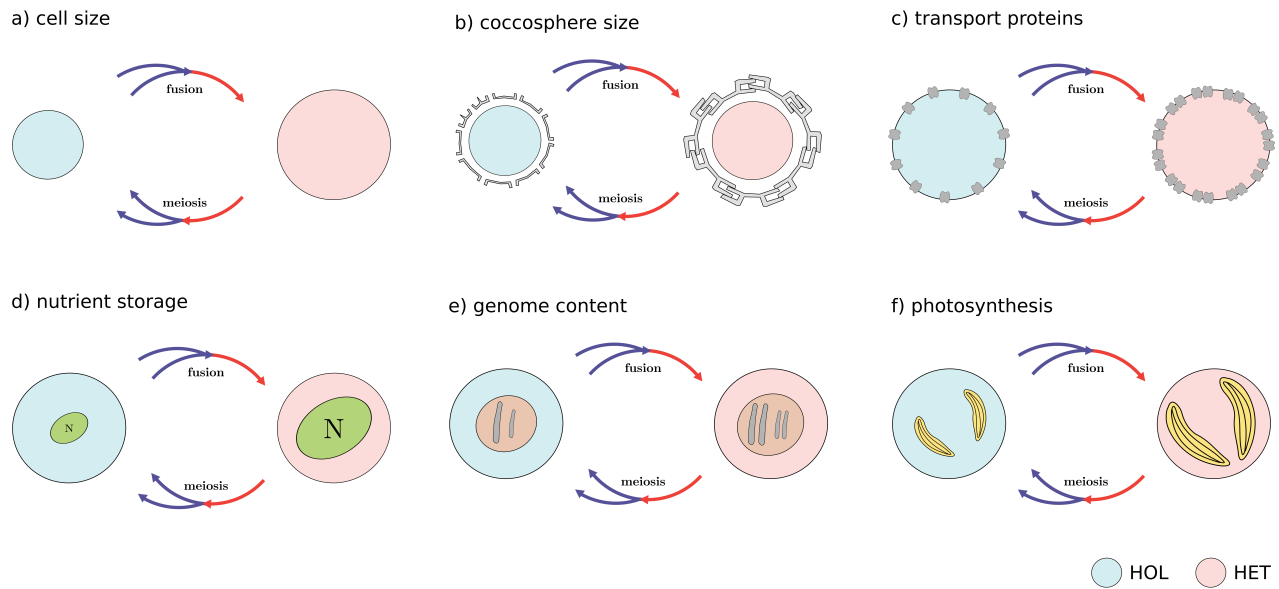
Figure A1. Main coccolithophore traits investigated in this study: **(a)** cell size; **(b)** coccosphere size; **(c)** transport proteins (nitrogen uptake rate); **(d)** nitrogen storage (maximum nitrogen quota); **(e)** genome content (nitrogen quota); **(f)** photosynthesis. Note that these are proposed trade-offs, and some trait differences were not observed in our study.
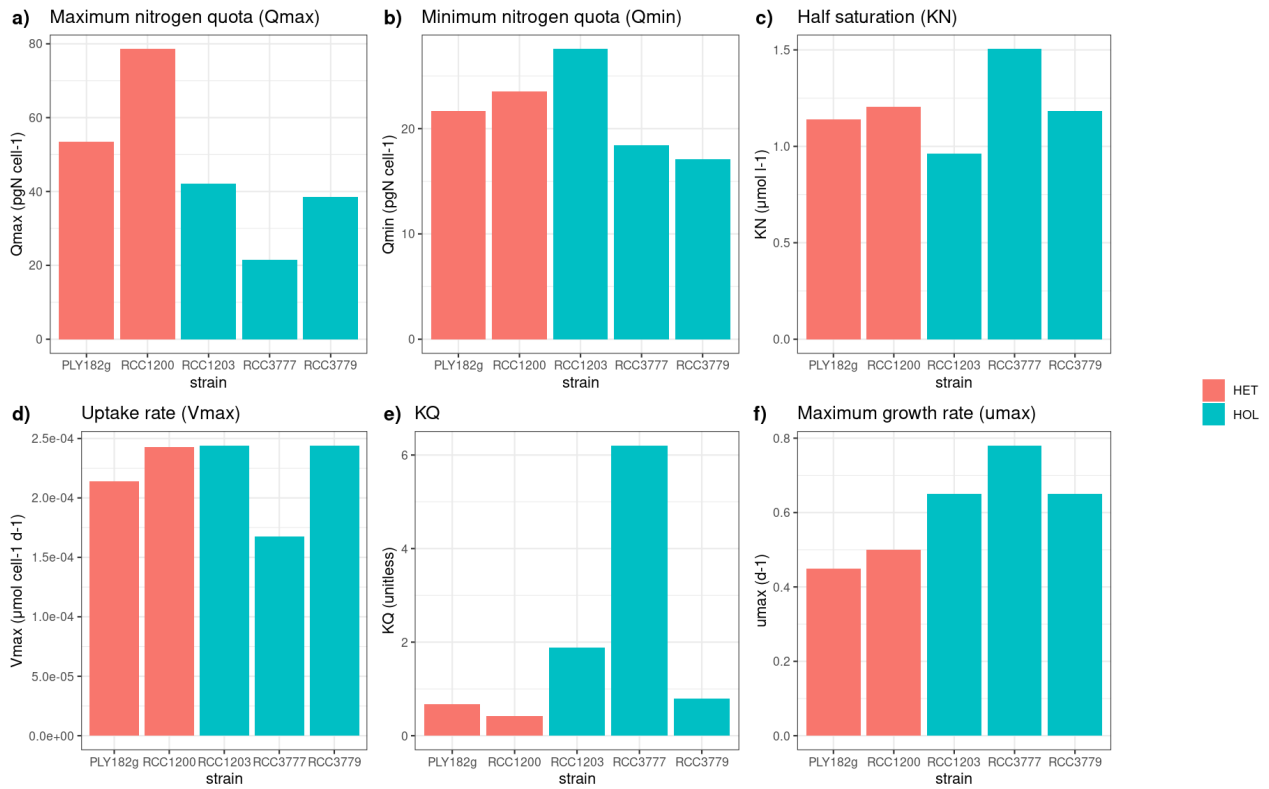
Figure A2. Estimated and measured model parameters. **(a)** maximum nitrogen quota (Q^{max}); **(b)** minimum nitrogen quota (Q^{min}); **(c)** half saturation constant (K_N); **(d)** uptake rate (V^{max}); **(e)** KQ; **(f)** maximum growth rate (μ^{max}).

Figure A3. Fluorescence data of temperature experiments used to estimate growth rates.
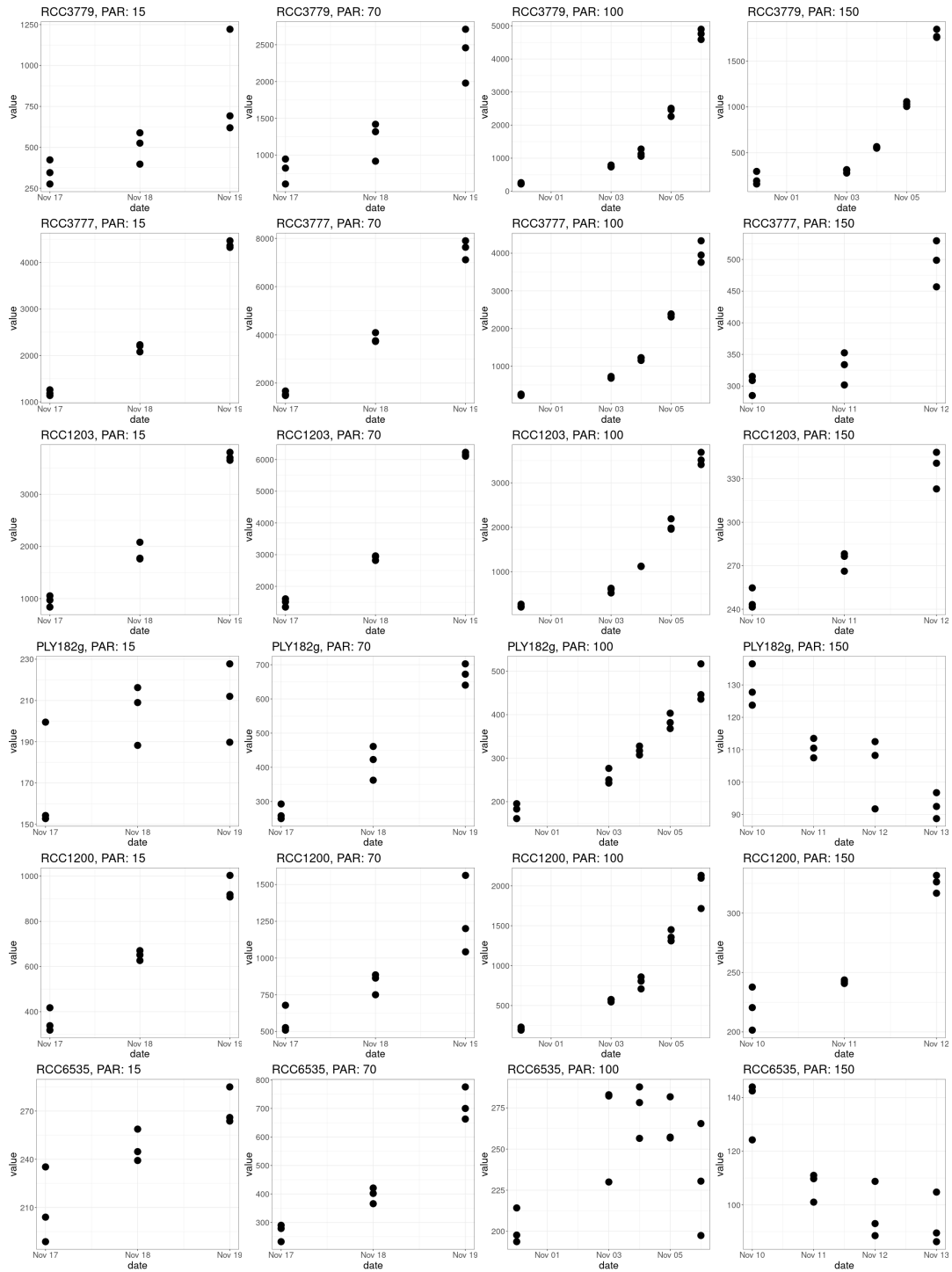
Figure A4. Fluorescence data of the first set of light experiments used to estimate growth rates.
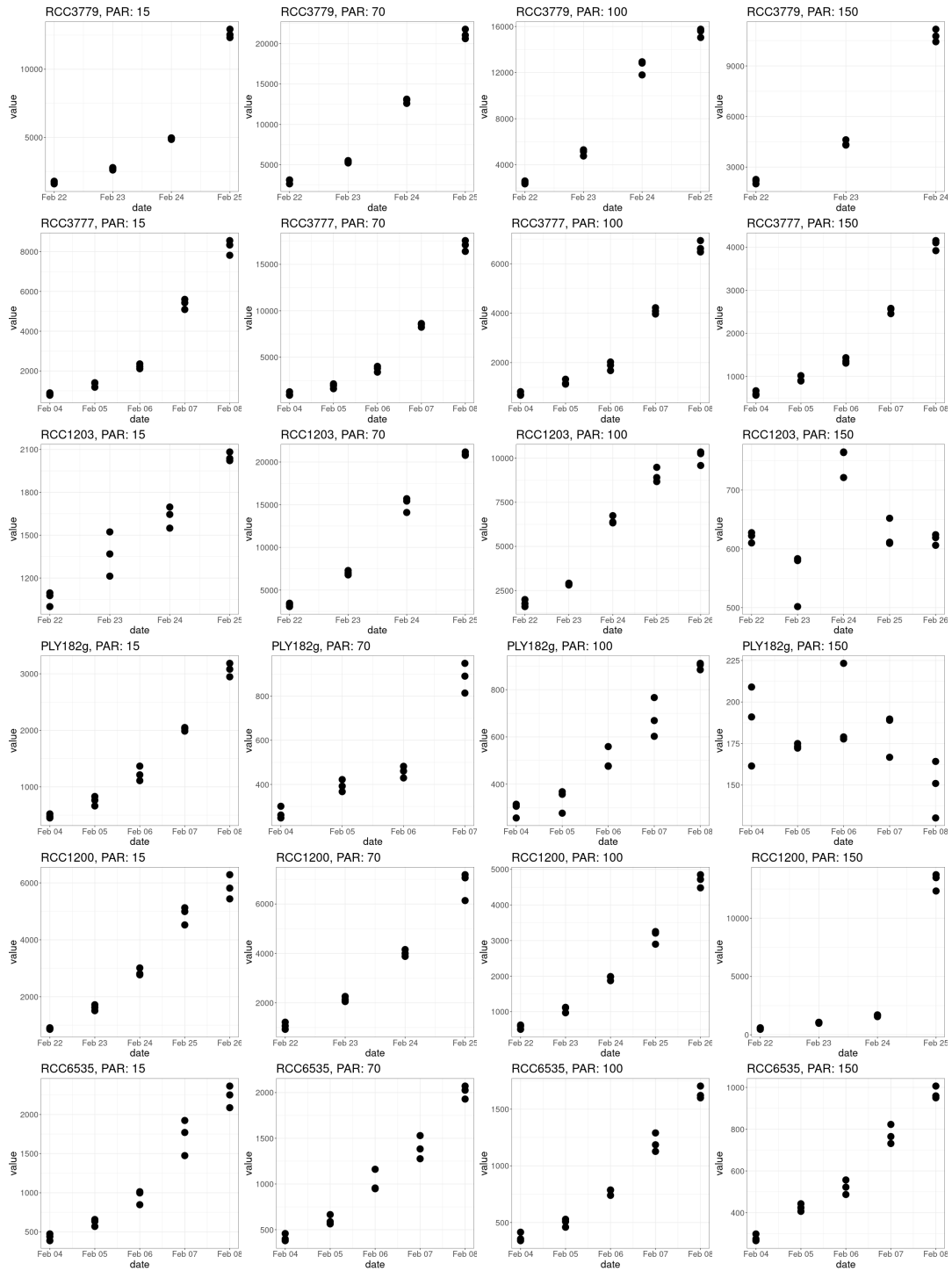
Figure A5. Fluorescence data of the second set of light experiments used to estimate growth rates.

Experiment	μ^{max} HET (d^{-1})	μ^{max} HOL (d^{-1})	Q^{max} HET (pgN cell^{-1})	Q^{max} HOL (pgN cell^{-1})	relative Q^{max} (unitless)	pulse intervals (d)
No cost	0.7	0.7	30	30	1	(0.5, 1, ..., 6)
No cost	0.7	0.7	37.5	30	1.25	(0.5, 1, ..., 6)
No cost	0.7	0.7	45	30	1.5	(0.5, 1, ..., 6)
No cost	0.7	0.7	52.5	30	1.75	(0.5, 1, ..., 6)
No cost	0.7	0.7	60	30	2	(0.5, 1, ..., 6)
No cost	0.7	0.7	90	30	3	(0.5, 1, ..., 6)
No cost	0.7	0.7	120	30	4	(0.5, 1, ..., 6)
Metabolic cost	0.5	0.7	30	30	1	(0.5, 1, ..., 6)
Metabolic cost	0.5	0.7	37.5	30	1.25	(0.5, 1, ..., 6)
Metabolic cost	0.5	0.7	45	30	1.5	(0.5, 1, ..., 6)
Metabolic cost	0.5	0.7	52.5	30	1.75	(0.5, 1, ..., 6)
Metabolic cost	0.5	0.7	60	30	2	(0.5, 1, ..., 6)
Metabolic cost	0.5	0.7	90	30	3	(0.5, 1, ..., 6)
Metabolic cost	0.5	0.7	120	30	4	(0.5, 1, ..., 6)

Table A1. Competition model experiments. Competition between HET and HOL cells was simulated with and without a metabolic cost (reduced μ^{max}). For each nutrient pulse interval, different ratios of HET and HOL Q^{max} (relative Q^{max}) were tested.

References

455 Avrahami, Y. and Frada, M. J.: Detection of Phagotrophy in the Marine Phytoplankton Group of the Coccolithophores (Calcihaptophycidae, Haptophyta) During Nutrient-replete and Phosphate-limited Growth, Journal of Phycology, 56, 1103–1108, https://doi.org/10.1111/jpy.12997, 2020.

Bach, L. T., Bauke, C., Meier, K. J., Riebesell, U., and Schulz, K. G.: Influence of changing carbonate chemistry on morphology and weight of coccoliths formed by Emiliania huxleyi, Biogeosciences, 9, 3449–3463, https://doi.org/10.5194/bg-9-3449-2012, 2012.

460 Boyd, P. W., Claustre, H., Levy, M., Siegel, D. A., and Weber, T.: Multi-faceted particle pumps drive carbon sequestration in the ocean, Nature, 568, 327–335, https://doi.org/10.1038/s41586-019-1098-2, 2019.

Cermeño, P., Lee, J. B., Wyman, K., Schofield, O., and Falkowski, P. G.: Competitive dynamics in two species of marine phytoplankton under non-equilibrium conditions, Marine Ecology Progress Series, 429, 19–28, https://doi.org/10.3354/meps09088, 2011.

Cros, L., Kleijne, A., Zeltner, A., Billard, C., and Young, J. R.: New examples of holococcolith–heterococcolith combination coccospheres
465 and their implications for coccolithophorid biology, 39, 1–5, 2000.

D'Amario, B., Ziveri, P., Grelaud, M., Oviedo, A., and Kralj, M.: Coccolithophore haploid and diploid distribution patterns in the Mediterranean Sea: Can a haplo-diploid life cycle be advantageous under climate change?, Journal of Plankton Research, 39, 781–794, https://doi.org/10.1093/plankt/fbx044, 2017.

Daniels, C. J., Tyrrell, T., Poulton, A. J., and Young, J. R.: A mixed life-cycle stage bloom of Syracosphaera bannockii(Borsetti and Cati,
470 1976) Cros et al . 2000 (Bay of Biscay, April 2010), Journal of Nannoplankton Research, 34, 31–35, 2014.

Daniels, C. J., Poulton, A. J., Young, J. R., Esposito, M., Humphreys, M. P., Ribas-Ribas, M., Tynan, E., and Tyrrell, T.: Species-specific calcite production reveals Coccolithus pelagicus as the key calcifier in the Arctic Ocean, Marine Ecology Progress Series, 555, 29–47, https://doi.org/10.3354/meps11820, 2016.

Dassow, P. V. and Montresor, M.: Unveiling the mysteries of phytoplankton life cycles: Patterns and opportunities behind complexity, Journal
475 of Plankton Research, 33, 3–12, https://doi.org/10.1093/plankt/fbq137, 2011.

Dassow, P. V., John, U., Ogata, H., Probert, I., Bendif, E. M., Kegel, J. U., Audic, S., Wincker, P., Silva, C. D., Claverie, J. M., Doney, S., Glover, D. M., Flores, D. M., Herrera, Y., Lescot, M., Garet-Delmas, M. J., and Vargas, C. D.: Life-cycle modification in open oceans accounts for genome variability in a cosmopolitan phytoplankton, ISME Journal, 9, 1365–1377, https://doi.org/10.1038/ismej.2014.221, 2015.

480 de Vries, J., Monteiro, F., Wheeler, G., Poulton, A., Godrijan, J., Cerino, F., Malinverno, E., Langer, G., and Brownlee, C.: Haplo-diplontic life cycle expands coccolithophore niche, Biogeosciences, 18, 1161–1184, https://doi.org/10.5194/bg-18-1161-2021, 2021.

Dormand, J. R. and Prince, P. J.: A family of embedded Runge-Kutta formulae, Journal of Computational and Applied Mathematics, 6, 19–26, https://doi.org/10.1016/0377-0427(86)90027-0, 1980.

Dutkiewicz, S., Morris, J. J., Follows, M. J., Scott, J., Levitan, O., Dyhrman, S. T., and Berman-Frank, I.: Impact of ocean acidification on
485 the structure of future phytoplankton communities, Nature Climate Change, 5, 1002–1006, https://doi.org/10.1038/nclimate2722, 2015.

Falkowski, P. G. and Oliver, M. J.: Mix and match: How climate selects phytoplankton, Nature Reviews Microbiology, 5, 813–819, https://doi.org/10.1038/nrmicro1751, 2007.

Fiorini, S., Middelburg, J. J., and Gattuso, J. P.: Effects of elevated CO2 partial pressure and temperature on the coccolithophore Syracosphaera pulchra, Aquatic Microbial Ecology, 64, 221–232, https://doi.org/10.3354/ame01520, 2011a.

490   Fiorini, S., Middelburg, J. J., and Gattuso, J. P.: Testing the effects of elevated pCO2 on coccolithophores (prymnesiophyceae): Comparison between haploid and diploid life stages, Journal of Phycology, 47, 1281–1291, https://doi.org/10.1111/j.1529-8817.2011.01080.x, 2011b.

Flynn, K. J.: How critical is the critical N:P ratio?, Journal of Phycology, 38, 961–970, https://doi.org/10.1046/j.1529-8817.2002.t01-1-01235.x, 2002.

Flynn, K. J.: The importance of the form of the quota curve and control of non-limiting nutrient transport in phytoplankton models, Journal

495   of Plankton Research, 30, 423–438, https://doi.org/10.1093/plankt/fbn007, 2008.

Follows, M. J. and Dutkiewicz, S.: Modeling diverse communities of marine microbes, Annual Review of Marine Science, 3, 427–451, https://doi.org/10.1146/annurev-marine-120709-142848, 2011.

Follows, M. J., Dutkiewicz, S., Grant, S., and Chisholm, S. W.: Emergent biogeography of microbial communities in a model ocean, Science, 315, 1843–1846, https://doi.org/10.1126/science.1138544, 2007.

500   Follows, M. J., Dutkiewicz, S., Ward, B. A., and Follett, C. N.: Theoretical interpretations of subtropical plankton biogeography, https://doi.org/10.1002/9780470281840, 2018.

Frada, M. J., Bendif, E. M., Keuter, S., and Probert, I.: The private life of coccolithophores, pp. 1–20, https://doi.org/10.1127/pip/2018/0083, 2018.

Fu, W., Randerson, J. T., and Moore, J. K.: Climate change impacts on net primary production (NPP) and export production (EP) reg-

505   ulated by increasing stratification and phytoplankton community structure in the CMIP5 models, Biogeosciences, 13, 5151–5170, https://doi.org/10.5194/bg-13-5151-2016, 2016.

Gal, A., Sorrentino, A., Kahil, K., Pereiro, E., Faivre, D., and Scheffel, A.: Native-state imaging of calcifying and noncalcifying microalgae reveals similarities in their calcium storage organelles, Proceedings of the National Academy of Sciences of the United States of America, 115, 11 000–11 005, https://doi.org/10.1073/pnas.1804139115, 2018.

510   Geider, R. J. and Roche, J. L.: Redfield revisited: Variability of C:N:P in marine microalgae and its biochemical basis, European Journal of Phycology, 37, 1–17, https://doi.org/10.1017/S0967026201003456, 2002.

Gerecht, A. C., Šupraha, L., Edvardsen, B., Probert, I., and Henderiks, J.: High temperature decreases the PIC / POC ratio and increases phosphorus requirements in Coccolithus pelagicus (Haptophyta), Biogeosciences, 11, 3531–3545, https://doi.org/10.5194/bg-11-3531-2014, 2014.

515   Gorbunov, M. Y. and Falkowski, P. G.: Using chlorophyll fluorescence kinetics to determine photosynthesis in aquatic ecosystems, Limnology and oceanography, 66, 1–13, 2021.

Grover, J. P.: Resource Competition in a Variable Environment: Phytoplankton Growing According to Monod's Model, The American Naturalist, 138, 811–835, 1991.

Hansen, P. J.: The size ratio between planktonic predators and their prey, Limnology and Oceanography, 39, 395–403, 1994.

520   Hansen, P. J., Bjørnsen, P. K., and Hansen, B. W.: Zooplankton grazing and growth: Scaling within the 2-2,000-μm body size range, Limnology and Oceanography, 42, 687–704, https://doi.org/10.4319/lo.1997.42.4.0687, 1997.

Houdan, A., Billard, C., Marie, D., Not, F., Sâez, A. G., Young, J. R., and Probert, I.: Holococcolithophore- heterococcolithophore (Haptophyta) life cycles: Flow cytometric analysis of relative ploidy levels, Systematics and Biodiversity, 1, 453–465, https://doi.org/10.1017/S1477200003001270, 2004.

525   Houdan, A., Probert, I., Lenning, K. V., and Lefebvre, S.: Comparison of photosynthetic responses in diploid and haploid life-cycle phases of Emiliania huxleyi (Prymnesiophyceae), Marine Ecology Progress Series, 292, 139–146, https://doi.org/10.3354/meps292139, 2005.

Houdan, A., Probert, I., Zatylny, C., Véron, B., and Billard, C.: Ecology of oceanic coccolithophores. I. Nutritional preferences of the two stages in the life cycle of Coccolithus braarudii and Calcidiscus leptoporus, Aquatic Microbial Ecology, 44, 291–301, https://doi.org/10.3354/ame044291, 2006.

530 Inomura, K., Omta, A. W., Talmy, D., Bragg, J., Deutsch, C., and Follows, M. J.: A Mechanistic Model of Macromolecular Allocation, Elemental Stoichiometry, and Growth Rate in Phytoplankton, Frontiers in Microbiology, 11, 1–22, https://doi.org/10.3389/fmicb.2020.00086, 2020.

Kiørboe, T.: Small-scale turbulence, marine snow formation, and planktivorous feeding, Scientia Marina, 61, 141–158, 1997.

Kiørboe, T., Visser, A., Andersen, K. H., and Browman, H.: A trait-based approach to ocean ecology, ICES Journal of Marine Science, 75,

535 1849–1863, https://doi.org/10.1093/icesjms/fsy090, 2018.

Kottmeier, D. M., Terbrüggen, A., Wolf-Gladrow, D. A., and Thoms, S.: Diel variations in cell division and biomass production of Emiliania huxleyi—Consequences for the calculation of physiological cell parameters, Limnology and Oceanography, 65, 1781–1800, https://doi.org/10.1002/lno.11418, 2020.

Kroon, D.: Numerical optimization of kernel based image derivatives, Short Paper University Twente, 3, 2009.

540 Laliberté, J., Bélanger, S., and Frouin, R.: Evaluation of satellite-based algorithms to estimate photosynthetically available radiation (PAR) reaching the ocean surface at high northern latitudes, Remote Sensing of Environment, 184, 199–211, 2016.

Langer, G., Jie, V. W., Kottmeier, D., Flori, S., Sturm, D., de Vries, J., Harper, G. M., Brownlee, C., and Wheeler, G.: Distinct physiological responses of Coccolithus braarudii life cycle phases to light intensity and nutrient availability, European Journal of Phycology, pp. 1–14, https://doi.org/10.1080/09670262.2022.2056925, 2022.

545 Liefer, J. D., Garg, A., Fyfe, M. H., Irwin, A. J., Benner, I., Brown, C. M., Follows, M. J., Omta, A. W., and Finkel, Z. V.: The macromolecular basis of phytoplankton C:N:P under nitrogen starvation, Frontiers in Microbiology, 10, 1–16, https://doi.org/10.3389/fmicb.2019.00763, 2019.

Litchman, E., Klausmeier, C. A., Schofield, O. M., and Falkowski, P. G.: The role of functional traits and trade-offs in structuring phytoplankton communities: Scaling from cellular to ecosystem level, Ecology Letters, 10, 1170–1181, https://doi.org/10.1111/j.1461-

550 0248.2007.01117.x, 2007.

Lomas, M. W. and Glibert, P. M.: Comparison of nitrate uptake, storage, and reduction in marine diatoms and flagellates, Journal of Phycology, 913, 903–913, 2000.

Malinverno, E., Triantaphyllou, M. V., Stavrakakis, S., Ziveri, P., and Lykousis, V.: Seasonal and spatial variability of coccolithophore export production at the South-Western margin of Crete (Eastern Mediterranean), Marine Micropaleontology, 71, 131–147,

555 https://doi.org/10.1016/j.marmicro.2009.02.002, 2009.

Margalef, R.: Life-forms of phytoplankton as survival alternatives in an unstable environment, Oceanologica Acta, 1, 493–509, https://doi.org/10.1007/BF00202661, 1978.

Maxwell, K. and Johnson, G. N.: Chlorophyll Fluorescence—a Practical Guide, Journal of Experimental Botany, 51, 659–668, 2000.

Monod, J.: The growth of bacterial cultures, Annual Reviews in M, 3, 371–394, 1949.

560 Monteiro, F. M., Bach, L. T., Brownlee, C., Bown, P., Rickaby, R. E., Poulton, A. J., Tyrrell, T., Beaufort, L., Dutkiewicz, S., Gibbs, S., Gutowska, M. A., Lee, R., Riebesell, U., Young, J., and Ridgwell, A.: Why marine phytoplankton calcify, Science Advances, 2, https://doi.org/10.1126/sciadv.1501822, 2016.

Passow, U. and Carlson, C. A.: The biological pump in a high CO2 world, Marine Ecology Progress Series, 470, 249–271, https://doi.org/10.3354/meps09985, 2012.

Perrin, L., Probert, I., Langer, G., and Aloisi, G.: Growth of the coccolithophore Emiliania huxleyi in light-And nutrient-limited batch reactors: Relevance for the BIOSOPE deep ecological niche of coccolithophores, Biogeosciences, 13, 5983–6001, https://doi.org/10.5194/bg-13-5983-2016, 2016.

Probert, I. and Houdan, A.: The Laboratory Culture of Coccolithophores, https://doi.org/https://doi.org/10.1007/978-3-662-06278-4, 2004.

R Core Team: R: A Language and Environment for Statistical Computing, R Foundation for Statistical Computing, Vienna, Austria, https://www.R-project.org/, 2022.

Rokitta, S. D., de Nooijer, L. J., Trimborn, S., de Vargas, C., Rost, B., and John, U.: Transcriptome analyses reveal differential gene expression patterns between the life-cycle stages of Emiliania huxleyi (haptophyta) and reflect specialization to different ecological niches, Journal of Phycology, 47, 829–838, https://doi.org/10.1111/j.1529-8817.2011.01014.x, 2011.

Smyth, T. J., Fishwick, J. R., Al-Moosawi, L., Cummings, D. G., Harris, C., Kitidis, V., Rees, A., Martinez-Vicente, V., and Woodward, E. M.: A broad spatio-temporal view of the Western English Channel observatory, Journal of Plankton Research, 32, 585–601, https://doi.org/10.1093/plankt/fbp128, 2010.

Steele, J. H. and Henderson, E. W.: The role of predation in plankton models, Journal of Plankton Research, 14, 157–172, https://doi.org/10.1093/plankt/14.1.157, 1992.

Sviben, S., Gal, A., Hood, M. A., Bertinetti, L., Politi, Y., Bennet, M., Krishnamoorthy, P., Schertel, A., Wirth, R., Sorrentino, A., Pereiro, E., Faivre, D., and Scheffel, A.: A vacuole-like compartment concentrates a disordered calcium phase in a key coccolithophorid alga, Nature Communications, 7, https://doi.org/10.1038/ncomms11228, 2016.

Tozzi, S., Schofield, O., and Falkowski, P.: Historical climate change and ocean turbulence as selective agents for two key phytoplankton functional groups, Marine Ecology Progress Series, 274, 123–132, https://doi.org/10.3354/meps274123, 2004.

Tyrrell, T.: The relative influences of nitrogen and phosphorus on oceanic primary production., Nature, 400, 525–531, 1999.

van der Walt, S., Schönberger, J. L., Nunez-Iglesias, J., Boulogne, F., Warner, J. D., Yager, N., Gouillart, E., Yu, T., and the scikit-image contributors: scikit-image: image processing in {P}ython, PeerJ, 2, e453, https://doi.org/10.7717/peerj.453, 2014.

Verdy, A., Follows, M., and Flierl, G.: Optimal phytoplankton cell size in an allometric model, Marine Ecology Progress Series, 379, 1–12, https://doi.org/10.3354/meps07909, 2009.

Villiot, N., Poulton, A. J., Butcher, E. T., Daniels, L. R., and Coggins, A.: Allometry of carbon and nitrogen content and growth rate in a diverse range of coccolithophores, Journal of Plankton Research, 43, 511–526, https://doi.org/10.1093/plankt/fbab038, 2021.

Virtanen, P., Gommers, R., Oliphant, T. E., Haberland, M., Reddy, T., Cournapeau, D., Burovski, E., Peterson, P., Weckesser, W., Bright, J., van der Walt, S. J., Brett, M., Wilson, J., Millman, K. J., Mayorov, N., Nelson, A. R. J., Jones, E., Kern, R., Larson, E., Carey, C. J., Polat, I., Feng, Y., Moore, E. W., VanderPlas, J., Laxalde, D., Perktold, J., Cimrman, R., Henriksen, I., Quintero, E. A., Harris, C. R., Archibald, A. M., Ribeiro, A. H., Pedregosa, F., van Mulbregt, P., and Contributors, S. .: {SciPy} 1.0: Fundamental Algorithms for Scientific Computing in Python, Nature Methods, 17, 261–272, https://doi.org/10.1038/s41592-019-0686-2, 2020.

Wales, D. J. and Doye, J. P.: Global optimization by basin-hopping and the lowest energy structures of Lennard-Jones clusters containing up to 110 atoms, Journal of Physical Chemistry A, 101, 5111–5116, https://doi.org/10.1021/jp970984n, 1997.

Ward, B. A., Wilson, J. D., Death, R. M., Monteiro, F. M., Yool, A., and Ridgwell, A.: EcoGEnIE 0.1: Plankton Ecology in the cGENIE Earth system model, Geoscientific Model Development Discussions, pp. 1–48, https://doi.org/10.5194/gmd-2017-258, 2017.

Widdicombe, C. E., Eloire, D., Harbour, D., Harris, R. P., and Somerfield, P. J.: Long-term phytoplankton community dynamics in the Western English Channel, Journal of Plankton Research, 32, 643–655, https://doi.org/10.1093/plankt/fbp127, 2010.

Wood, S. N.: Fast stable restricted maximum likelihood and marginal likelihood estimation of semiparametric generalized linear models, Journal of the Royal Statistical Society (B), 73, 3–36, 2011.

Young, J. R., Geisen, M., Cros, L., Kleijne, A., Sprengel, C., Probert, I., and Østergaard, J.: A guide to extant coccolithophore taxonomy, Journal of Nannoplankton Research, p. 125, 2003.

Zeebe, R. E.: LOSCAR: Long-term Ocean-atmosphere-Sediment CArbon cycle Reservoir model v2.0.4, Geoscientific Model Development, 5, 149–166, https://doi.org/10.5194/gmd-5-149-2012, nULL, 2012.

Zwietering, M. H., Jongenburger, I., Rombouts, F. M., and van't Riet, K.: Modeling of the Bacterial Growth Curve, Applied and environmental microbiology, 56, 1875–1881, https://doi.org/10.1016/j.fm.2004.01.007, 1990.

605